HHS Public Access

Author manuscript

Nanoscale. Author manuscript; available in PMC 2018 August 31.

Published in final edited form as:

Nanoscale. 2017 August 31; 9(34): 12609–12617. doi:10.1039/c7nr03086j.

Ultra-small iron-gallic acid coordination polymer nanoparticles for chelator-free labeling of ^{64}Cu and multimodal imaging-guided photothermal therapy†

Qiutong Jin[a], **Wenjun Zhu**[a], **Dawei Jiang**[b,c], **Rui Zhang**[a], **Christopher J. Kutyreff**[b], **Jonathan W. Engle**[b], **Peng Huang**[c], **Weibo Cai**[b], **Zhuang Liu**[a], and **Liang Cheng**[a]

[a]Institute of Functional Nano & Soft Materials (FUNSOM), College of Nano Science & Technology (CNST), Collaborative Innovation Center of Suzhou Nano Science and Technology, Soochow University, Suzhou, Jiangsu 215123, China

[b]Departments of Radiology and Medical Physics, University of Wisconsin-Madison, Wisconsin 53705, USA

[c]Guangdong Key Laboratory for Biomedical Measurements and Ultrasound Imaging, School of Biomedical Engineering, Health Science Center, Shenzhen University, Shenzhen 518060, China

Abstract

Cancer nanotechnology has become the hot topic nowadays. While various kinds of nanomaterials have been widely explored for innovative cancer imaging and therapy applications, safe multifunctional nano-agents without long-term retention and toxicity are still demanded. Herein, iron-gallic acid coordination nanoparticles (Fe-GA CPNs) with ultra-small sizes are successfully synthesized by a simple method for multimodal imaging-guided cancer therapy. After surface modification with polyethylene glycol (PEG), the synthesized Fe-GA-PEG CPNs show high stability in various physiological solutions. Taking advantage of high near-infrared (NIR) absorbance as well as the T_1-MR contrasting ability of Fe-GA-PEG CPNs, *in vivo* photoacoustic tomography (PAT) and magnetic resonance (MR) bimodal imaging are carried out, revealing the efficient passive tumor targeting of these ultra-small CPNs after intravenous (i.v.) injection. Interestingly, such Fe-GA-PEG CPNs could be labeled with the ^{64}Cu isotope *via* a chelator-free method for *in vivo* PET imaging, which also illustrates the high tumor uptake of Fe-GA CPNs. We further utilize Fe-GA-PEG CPNs for *in vivo* photothermal therapy and achieve highly effective tumor destruction after i.v. injection of Fe-GA-PEG CPNs and the following NIR laser irradiation of the tumors, without observing any apparent toxicity of such CPNs to the treated animals. Our work highlights the promise of ultra-small iron coordination nanoparticles for imaging-guided cancer therapy.

†Electronic supplementary information (ESI) available. See DOI: 10.1039/ c7nr03086j

Correspondence to: Weibo Cai; Liang Cheng.

Introduction

Cancer has become one of the leading causes of death nowadays.[1–3] Traditional cancer treatments, such as surgery, chemotherapy, and radiotherapy have been extensively adopted for clinical cancer therapy. However, these therapeutic modalities inevitably cause serious side effects and often show low therapeutic efficacy. With the development of nanotechnology, new types of non-invasive and effective cancer treatment methods are emerging as powerful techniques for cancer therapy.[4–6] For instance, photothermal therapy (PTT), which employs near-infrared (NIR) light-absorbing agents to generate heat from optical energy and lead to thermal ablation of cancer cells, has received tremendous interest in nano-medicine.[4] Various inorganic/organic nanomaterials including carbon-based nanomaterials,[7,8] gold-based nanomaterials,[9–14] metallic nanoparticles,[15,16] black phosphorus,[17,18] transition metal dichalcogenides,[19–24] and organic nanomaterials[25,26] have shown great potential for photothermal cancer treatment due to their unique physiochemical properties. On the other hand, imaging-guided cancer therapy for better therapeutic planning and monitoring of therapeutic responses has been proposed to realize personalized therapy.[11,27–30] Despite encouraging results for the use of different types of nano-agents for imaging-guided photothermal ablation of cancer cells, the potential safety concerns remain a major problem that hampers the future clinical use of many nano-agents, especially non-biodegradable ones.

Coordination polymer-based nanoparticles (CPNs), also known as nano-sized metal–organic coordination nano-particles or nanoscale metal–organic frameworks, are a class of hybrid materials formed by the self-assembly between metal ions or clusters and organic polydentate bridging ligands. Recently, CPNs have been widely used in nanomedicine due to their attractive advantages of biodegradability, easy surface modification, as well as their capability of loading of various imaging and therapeutic molecules.[31–37] Notably, it has been demonstrated that coordination polymer-based nanoparticles exhibit inherent biocompatibility, and could be gradually degraded and efficiently excreted from the body without rendering long-term retention and toxicity concerns.[38–40] Therefore, it would be of great interest to design new types of CPNs for imaging-guided cancer therapy.

In this work, we used a simple one-step assembly method to synthesize phenolic group-metal ion coordination nanoparticles on a large scale and used them for multimodal imaging-guided photothermal therapy. By simply mixing a $FeCl_3$ solution with a gallic acid (GA) solution, ultra-small Fe-GA coordination nanoparticles (CPNs) with the size of 5 nm were formed and their surface could be modified with polyethylene glycol (PEG). Interestingly, the synthesized Fe-GA-PEG CPNs could be labeled with the ^{64}Cu isotope (with the half time of 12 h) *via* a chelator-free method by simply mixing, yielding ^{64}Cu-Fe-GA-PEG CPNs with a high labeling yield and high serum/*in vivo* stability. Compared with the ^{64}Cu-Fe-GA CPNs without a PEG coating, much more efficient passive tumor accumulation of ^{64}Cu-Fe-GA-PEG CPNs was observed after intravenous (i.v.) injection into tumor-bearing mice. In addition, *in vivo* photoacoustic tomography (PAT) and magnetic resonance (MR) bimodal imaging, by taking advantage of strong NIR absorbance and the T_1-MR contrasting ability of Fe-GA-PEG CPNs, respectively, further evidence the efficient passive tumor targeting of these ultra-small CPNs after i.v. injection. We further utilized Fe-

GA-PEG CPNs for *in vivo* photothermal therapy and achieved highly effective tumor destruction after i.v. injection of Fe-GA-PEG CPNs and the following NIR laser irradiation of the tumors. No appreciable toxicity was observed for Fe-GA-PEG, to the treated animals. Our results, for the first time, report Fe-GA coordination nanoparticles for chelator-free labeling and PET imaging, together with MR/PAT dual modal imaging functions, to guide the high-performance photothermal ablation of tumors, highlighting the great potential of coordination nanoparticles in cancer theranostics.

Experiment section

Synthesis of Fe-GA coordination nanoparticles (CPNs)

The Fe-GA CPNs were synthesized according to previous studies.[40,41] In brief, 100 mg of polyvinylpyrrolidone (PVP) was dissolved in 10 ml of water at room temperature under vigorous stirring. An $FeCl_3$ aqueous solution (0.2 ml, 100 mg mL^{-1}) was then added to the aqueous PVP solution. After 1 h of incubation, a GA aqueous solution (1 ml, 10 mg mL^{-1}) was added to the above reaction mixture and stirred overnight. The resulting coordination polymer nanoparticles were dialyzed (MWCO = 14 800) against deionized water for 24 h and stored in a refrigerator for further use.

PEGylated Fe-GA CPNs

By utilizing the carboxyl group of the GA molecule, the surface of the Fe-GA CPNs could be modified with amine-terminated PEG by amide formation. A solution of mPEG-amine (Sunbio Inc., M_w = 5 kDa) at 10 mg mL^{-1} was added into the Fe-GA CPN solution (2 mg mL^{-1}) and the mixture was sonicated for half an hour. 5 mg *N*-(3-dimethylaminopropyl-*N*′-ethylcarbodi-imide) hydrochloride (EDC, Fluka Inc.) was then added to the mixture with pH adjusted to 8. The reaction was conducted overnight, yielding Fe-GA-PEG CPNs, which were purified by washing and stored at 4 °C for future use.

Characterization

Transmission electron microscopy (TEM) images of the nanostructures were obtained using an FEI Tecnai F20 transmission electron microscope. The hydrodynamic diameters of Fe-GA and Fe-GA-PEG CPNs were determined by using a Zetasizer Nano-ZS (Malvern Instruments, UK). The concentrations of each metal ion were measured *via* inductively coupled plasma optical emission spectroscopy (ICP-OES, Thermo). The infrared spectrum was captured by using a Bruker Hyperion FTIR spectrometer.

Cell culture experiments

Murine breast cancer cells (4T1), mouse fibroblast cells (NIH3T3), and human glioblastoma cells (U87MG) were obtained from American Type Culture Collection (ATCC) and cultured at 37 °C under 5% CO_2. All cell culture related reagents were purchased from Invitrogen. 4T1 cells were cultured in standard RPMI-1640 medium containing 10% fetal bovine serum (FBS) and 1% penicillin/streptomycin. NIH3T3 and U87MG cells were cultured in DMEM low-glucose medium containing 10% fetal bovine serum and 1% penicillin/streptomycin. Cells were seeded into 96-well plates at a density of 1×10^4 cells per well and incubated

with different concentrations of Fe-GA-PEG CPNs for 24 h. Relative cell viabilities were determined by the standard methyl thiazolyl tetrazolium (MTT) assay.

In vitro photothermal therapy

For *in vitro* PTT, 4T1 cells (1×10^4) were seeded in 96-well plates and added with Fe-GA-PEG CPNs at various concentrations. After incubation for 24 h, the experimental groups were exposed to 808 nm laser irradiation under a power density of 1 W cm^{-2} for 5 min, while the control group was still cultured in the dark. Afterward, the MTT assay was carried out following the standard protocol. After laser irradiation, cells were washed with phosphate buffered saline (PBS) and stained with 0.4% Trypan blue (Sigma) before imaging by using a confocal fluorescence microscope (Leica SP5).

^{64}Cu labeling

^{64}Cu was produced with an onsite cyclotron (GE PETtrace). Briefly, $^{64}CuCl_2$ (~150 MBq) was diluted in 300 μL of 0.1 M sodium acetate buffer (pH 5.5) and mixed with 100 μL of Fe-GA-PEG CPNs (0.5 mg mL^{-1}). The reaction was conducted at 37 °C for 60 min with constant shaking. The labeling yield was determined by thin-layer chromatography (TLC) at different time points. The resulting ^{64}Cu-Fe-GA-PEG CPNs were purified using PD-10 columns with PBS as the mobile phase. In contrast, Fe-GA CPNs without PEG coating also labeled with ^{64}Cu using the same method. A serum stability study was carried out to ensure that ^{64}Cu was stably attached on Fe-GA-PEG CPNs. ^{64}Cu-Fe-GA-PEG CPNs were incubated in PBS and whole serum at 37 °C for up to 24 h. At different time points, portions of the mixture were sampled and filtered through 5 kDa MWCO filters. The retained (*i.e.*, intact) ^{64}Cu on ^{64}Cu-Fe-GA-PEG CPNs was calculated using the equation (radioactivity on filter/total sampled radioactivity × 100%).

Tumor models

All animal studies were conducted according to the protocols approved by the Soochow University Laboratory Animal Center and the University of Wisconsin Institutional Animal Care and Use Committee. The 4T1 subcutaneous xenografts were generated by subcutaneous injection of 1×10^6 cells in ~30 μL RMPI-1640 medium onto the back of each female Balb/c mice. The mice were used when tumor volumes reached about ~70 mm^3.

In vivo PET imaging

For PET imaging, 4T1 tumor-bearing mice (3 mice per group), post intravenous (i.v.) injection of ~10 MBq of ^{64}Cu-Fe-GA-PEG CPNs, were imaged using a microPET/microCT Inveon rodent model scanner (Siemens Medical Solutions USA, Inc.). Data acquisition, image reconstruction, and ROI analysis of the PET data were performed as described previously.[42] At the same time, ^{64}Cu-Fe-GA CPNs without PEG coating were also intravenously injected into the tumor-bearing mice and imaged using the same PET/CT model scanner as for the control. After the PET scans at 24 h, *ex vivo* biodistribution studies were carried out to ensure that the %ID g^{-1} values determined by PET imaging actually represented the radioactivity distribution in the tumor-bearing mice. The mice were euthanized, and blood, tumors, and major organs/tissues were collected and wet-weighed.

The radioactivity in these tissues was measured using a gamma-counter (PerkinElmer, USA) and presented as %ID g^{-1} (mean ± SD).

MR&PAT imaging

The longitudinal (T_1) and transverse (T_2) relaxation times of the Fe-GA-PEG CPNs were measured using a 1 T MicroMR-25 mini MR system (Niumag Corporation, Shanghai, China) at 25 °C. The measurement parameters were as follows: T_1-weighted sequence, spin echo, TR/TE = 500/18.2 ms, matrix acquisition = 90 × 90, NS = 2, FOV = 80 mm × 80 mm, slices = 8, slice width = 5.0 mm, slice gap = 0.55 mm, 0.55 T, 32.0 °C. Relaxivity values (r_1 and r_2) were calculated by fitting the $1/T_1$ and $1/T_2$ relaxation times (S^{-1}) *versus* Fe^{3+} concentration (mM) curves.

For T_1-MR imaging, the tumor-bearing mice were intravenously injected with Fe-GA-PEG CPNs (200μl, 2 mg mL^{-1}). T_1-Weighted MR images were recorded on a 3T clinical MRI scanner (Bruker Biospin Corporation, Billerica, MA, USA) equipped with a small animal imaging coil. T_1-Weighted images were acquired using the following parameters: TR, 2000 ms; TE, 106.4 ms; slice thickness, 2.0 mm; slice spacing, 0.2 mm; matrix, 224 × 192; FOV, 10 cm × 10 cm.

PAT imaging was performed with a Visualsonic Vevo® 2100 LAZER system. During the experiments, anesthesia was maintained using isoflurane. The body temperature of the mice was maintained by using a water heating system at 37.5 °C. The 4T1 tumor-bearing mice were intravenously injected with Fe-GA-PEG CPNs solution before imaging (2 mg mL^{-1}, 200 μL).

In vivo photothermal therapy

After the tumor volume reached ~70 mm^3, the mice were randomly divided into four groups (n = 5 per group) for various treatments: control (i), Fe-GA-PEG CPNs injected (ii), laser only (iii), Fe-GA-PEG CPNs + laser (iv). Fe-GA-PEG CPNs at the dose of 20 mg kg^{-1} was intravenously injected into mice bearing 4T1 tumors. An optical fiber coupled 808 nm high power diode-laser (Hi-Tech Optoelectronics Co., Ltd, Beijing, China) was used to irradiate the tumors during our experiments. For photothermal treatment, the laser beam with a diameter of ~10 mm was focused on the tumor area at the power density of 1 W cm^{-2} for 5 minutes. Infrared thermal images were taken by using an IRS E50 Pro Thermal Imaging Camera. The tumor sizes were measured by using a caliper every the other day and calculated as the volume = (tumor length) × (tumor width)^2/2. Relative tumor volumes were calculated as V/V_0 (V_0 was the tumor volume when the treatment was initiated).

Histology analysis

30 days after injection of Fe-GA-PEG CPNs (dose = 20 mg kg^{-1}), 3 mice from the treatment group and 3 age-matched female Balb/c control mice (without injection of Fe-GA-PEG CPNs) were sacrificed by CO_2 asphyxiation for necropsy. The major organs from those mice were harvested, fixed in 10% neutral buffered formalin, processed routinely in paraffin, sectioned at 8 microns, stained with hematoxylin & eosin (H&E) and examined by using a

digital microscope (Leica QWin). The examined tissues include liver, spleen, kidney, heart, lung and intestine.

Results and discussion

Fe-GA coordination polymer nanoparticles (CPNs) were obtained by mixing the $FeCl_3$ solution with gallic acid (GA) in the presence of PVP (Fig. 1a). GA is a type of tea-polyphenol that can react with Fe^{3+} to form a stable GAn–Fe^{3+} complex *via* the formation of Fe^{3+}–phenolate carboxylate coordination bonds. Firstly, the PVP–Fe^{3+} compound formed when mixing the PVP and $FeCl_3$ solution. The PVP polymer itself not only acts as a metal chelating agent but also serves as a protecting polymer during the nucleation and growth processes of the coordination polymer nanodots (CPNs). From the FTIR spectra, we could find that the infrared intensity of the Fe-GA CPNs at 1250 cm^{-1} (the HO–C stretching band) was lower than that of GA, indicating that the HO–C phenolic hydroxyl group of GA coordinated with Fe^{3+} (ref. 40) (ESI Fig. S1†). From the transmission electronic microscopy (TEM) imaging, the as-synthesized Fe-GA showed the regular size of ~5 nm (ESI Fig. S2†). Although as-synthesized Fe-GA CPNs coated with PVP were soluble in water, they would rapidly aggregate in the presence of salts after removal of the excess PVP (ESI Fig. S3†). Therefore, we used the amine-terminated PEG polymer to modify the synthesized Fe-GA CPNs through a simple EDC-triggered chemical coupling method. Fig. 1b shows the transmission electronic microscopy (TEM) images of the PEGylated Fe-GA CPNs with uniform and ultra-small size. After PEG coating, the sizes of Fe-GA-PEG CPNs measured by dynamic light scattering (DLS) showed a slight increase to ~20 nm for the final product (Fig. 1c). Such Fe-GA-PEG CPNs exhibited remarkably improved stability, without showing any sign of aggregation even after several days of incubation in various physiological solutions including water, saline, cell medium, and serum (Fig. 1d inset), suggesting successful PEGylation on the surface of those Fe-GA CPNs (ESI Fig. S4†).

The UV-vis-NIR spectra of Fe-GA-PEG CPNs showed high absorbance in a wide spectrum range from 700–1000 nm. Under the 808 nm NIR laser irradiation, Fe-GA-PEG CPNs showed clear concentration-dependent temperature increases. The temperature of the Fe-GA-PEG CPNs with a concentration of 0.8 mg mL^{-1} could increase by 20 °C after laser irradiation for 5 min (808 nm laser at 0.8 W cm^2), while pure water showed an only 3 °C increase under the same conditions. Also, the photothermal performance remained rather stable after five cycles of NIR laser irradiation (ESI Fig. S5†). These results together suggested that Fe-GA-PEG CPNs would be an effective photothermal agent for cancer therapy.

To explore the applications of Fe-GA-PEG CPNs in biomedicine, firstly we tested their potential toxicity to several types of cells. The standard methyl thiazolyl tetrazolium (MTT) assay was carried out to determine the relative viabilities of murine breast cancer cells (4T1), mouse fibroblast cells (NIH3T3), and human glioblastoma cells (U87MG) after they were incubated with Fe-GA-PEG CPNs at various concentrations for 24 h. No significant

†Electronic supplementary information (ESI) available. See DOI: 10.1039/ c7nr03086j

cytotoxicity of Fe-GA-PEG CPNs was observed for all three types of cells even at high concentrations up to 0.4 mg mL^{-1} (Fig. 2a).

Next, we used Fe-GA-PEG CPNs as the photothermal agent for *in vitro* cancer cell ablation under laser irradiation. 4T1 cells were incubated with various concentrations of Fe-GA-PEG CPNs for 24 h and then irradiated by the 808 nm laser with a power density of 1 W cm^{-2}. The MTT assay was also performed to quantitatively measure the relative cell viabilities after PTT treatment under different concentrations (Fig. 2b). It was determined that with the increase in Fe-GA-PEG concentrations, more cells were killed after the laser irradiation. The majority of cells were destroyed after being incubated with 0.4 mg mL^{-1} of Fe-GA-PEG CPNs and exposed to the NIR laser at 1 W cm^{-2} for 5 min. In contrast, the cells without Fe-GA-PEG CPNs incubation were not affected even after laser exposure. Following laser irradiation, the cells were further stained using Trypan blue. The cells in the control groups showed no color change, confirming that Fe-GA-PEG CPN incubation alone was not harmful to the cells. Upon laser irradiation, most cells incubated with Fe-GA-PEG CPNs at the concentration of 0.4 mg mL^{-1} were killed, as indicated by the intense homogeneous blue color (Fig. 2c). All these findings together revealed that Fe-GA-PEG CPNs hold great promise as an effective photothermal agent for tumor therapy.

To optimize the treatment planning and monitor the therapeutic responses, imaging-guided therapy has been proposed as an encouraging strategy to realize personalized medicine. Among all diagnostic imaging methods, radionuclide-based positron emission tomography (PET) has unique advantages of high sensitivity and the ability to conduct the quantitative analysis of whole-body images. However, chelator molecules like 1,4,7-triazacyclononane-1,4,7-triacetic acid (NOTA), 1,4,7,10-tetraazacyclododecane-1,4,7,10-tetraacetic acid (DOTA), or *p*-iso-thiocyanatobenzyl desferrioxamine B (DFO) usually need to be conjugated to bimolecular or nanoparticles for radiolabeling,[43] which sometimes would influence the surface properties of the materials and reduce the capability of loading other targeting or therapeutic agents. Thus, chelator-free radiolabeling techniques as alternative methods to label nanoparticles would be quite attractive.[44] Motivated by the high affinity between iron and the phenolic hydroxyl groups of GA, we thus hypothesized that Fe-GA CPNs may be labeled with ^{64}Cu in a chelator-free manner (Fig. 3a). By simply mixing $^{64}CuCl_2$ with Fe-GA-PEG CPNs at 37 °C for 1 h under constant shaking, we found that $^{64}Cu^{2+}$ was immediately adsorbed by Fe-GA-PEG CPNs (^{64}Cu-Fe-GA-PEG) as detected by thin-layer chromatography (TLC). The labeling yield was measured to be as high as 75% after 1 h of incubation (Fig. 3b and c). Moreover, the ^{64}Cu labeling of ^{64}Cu-Fe-GA-PEG CPNs was highly stable in mouse serum for 24 h at 37 °C (Fig. 3d). Such highly efficient and stable chelator-free labeling of ^{64}Cu-Fe-GA-PEG CPNs would be suitable for *in vivo* PET imaging.

The 4T1 tumor-bearing mice were imaged using a microPET Inveon rodent model scanner at various time points post i.v. injection of ^{64}Cu-Fe-GA-PEG CPNs (~10 MBq). Interestingly, these CPNs showed an efficient time-dependent tumor accumulation after the injection (Fig. 4a). Quantitative data obtained from region-of-interest (ROI) analysis of these PET images revealed the tumor uptake of the ^{64}Cu-Fe-GA-PEG CPNs to be 6.75 ± 1.02, 7.25 ± 1.13, 7.42 ± 1.22, and 6.95 ± 1.32 %ID g^{-1} at 1 h, 2 h, 4 h, and 24 h post-injection

(p.i., Fig. 4c), respectively ($n = 3$). In contrast, for the mice with i.v. injection of ^{64}Cu-Fe-GA without PEG coating, the tumor uptake was much lower at all the measured time points (1.85 ± 0.61, 2.43 ± 0.84, 3.95 ± 0.72, and 3.62 ± 0.98 %ID g^{-1} at 1 h, 2 h, 4 h, and 24 h p.i., respectively, Fig. 4b). Such an efficient passive tumor homing of the ultra-small Fe-GA-PEG CPNs could be attributed to the surface modification with PEG that leads to more effective enhancement of the permeability and retention (EPR) effect.

To further confirm the accuracy of PET quantification analysis, *ex vivo* biodistribution studies were carried out at 24 h for these two groups. As shown in Fig. 5, the tumor uptake of ^{64}Cu-Fe-GA CPNs at 24 h p.i. with values of 5.0 ± 1.2 %ID g^{-1} was slightly higher than that without PEG coating at 24 h post injection with values of 3.6 ± 0.5 %ID g^{-1}. The quantitative results based on PET and biodistribution studies appeared to be consistent, indicating that serial non-invasive PET imaging accurately reflected the distribution of Fe-GA CPNs in the 4T1 tumor-bearing mice.

Photoacoustic tomography (PAT), which is based on the photoacoustic effect of light-absorbers, offers remarkably increased imaging depth and spatial resolution compared with traditional *in vivo* optical imaging.[45] With strong NIR absorbance, Fe-GA CPNs could also serve as a contrast agent for *in vivo* PA imaging. The mice bearing 4T1 tumors were i.v. injected with Fe-GA-PEG CPNs (2 mg mL^{-1}, 200 μL) and imaged under a PA imaging system (excitation wavelength = 800 nm). As shown in Fig. 6a, the initial PA signal in the tumor site before injection was rather weak. After injection of Fe-GA-PEG CPNs, the PA signal in the tumor tissue became stronger due to the passive tumor accumulation of CPNs (Fig. 6c). The whole tumor was brightened up, later on, indicating that a large amount of Fe-GA-PEG CPNs was homogenously accumulated inside the tumor.

In the structure of Fe-GA CPNs, Fe^{3+} is oxygen-bonded with a high-spin ($S = 5/2$). Therefore, the compound may have the ability to shorten the longitudinal and transverse relaxation times (T_1 or T_2) of protons from bulk water. We determined the longitudinal and transverse relaxivities (r_1 and r_2 values, respectively) of the Fe-GA-PEG CPNs under serial dilutions under the MR scanner. The concentration-normalized relaxivity values were measured to be r_1= 3.5 mM^{-1} S^{-1}, and r_2 = 0.97 mM^{-1} S^{-1}, with the r_2/r_1 = 0.28 (ESI Fig. S6†). These results were in excellent agreement with those reported in the literature.[40] With a relatively high r_1 relaxivity and a low r_2/r_1 ratio, Fe-GA-PEG CPNs may serve as great T_1-weighted MR contrast agents. The mice bearing 4T1 tumors were i.v. injected with Fe-GA-PEG CPNs (dose = 20 mg kg^{-1}) and imaged by using a 3 T clinical MR scanner equipped with a small animal imaging coil. A remarkable brightening effect in the tumors of the injected mice was observed after 24 h (Fig. 6b and d), also suggesting the high passive tumor uptake of Fe-GA-PEG CPNs *via* the EPR effect of cancerous tumors. From the above results, our synthesized Fe-GA CPNs could be successfully used as a PA/MRI/PET tri-modal imaging contrast agent. Each imaging modality has its own unique advantages along with intrinsic limitations. The combination of those different imaging modalities would be of great importance to provide valuable information with high sensitivity and high resolution, helping physicians design better therapeutic approaches for the treatment of cancer.

Encouraged by the high tumor accumulation of Fe-GA-PEG CPNs and strong capability to induce *in vitro* PTT, we performed *in vivo* PTT experiments to confirm the efficacy of the ultra-small nanoparticles. After being intravenously injected with Fe-GA-PEG CPN solutions (2 mg mL^{-1}, 200 μL for each mouse) for 24 h, the mice bearing 4T1 tumors were anesthetized and exposed to an 808 nm laser with different power densities. Infrared (IR) thermal mapping apparatus was used to record the temperature change in the tumor area under NIR irradiation (Fig. 7). In mice i.v. injected with Fe-GA-PEG CPNs, their tumor surface temperature rapidly increased from ~25 °C to ~60 °C within 5 min of laser irradiation (1 W cm^{-2}, 5 min). In comparison, the tumor temperature of the mice without Fe-GA-PEG CPN injection under the same irradiation conditions showed little change.

Finally, the *in vivo* therapeutic efficacy of Fe-GA-PEG CPN induced PTT cancer treatment was studied. Five mice bearing 4T1 tumors on their back were i.v. injected with Fe-GA-PEG CPNs (2 mg mL^{-1}, 200 μL). At 24 h p.i., the tumor of each mouse in the treatment group was exposed to an 808 nm laser at a power density of 1 W cm^{-2} for 5 min. Three other groups including untreated mice (control, $n = 5$), mice exposed to the laser (laser only, $n = 5$), and Fe-GA-PEG CPNs injected mice without laser irradiation (Fe-GA-PEG, $n = 5$), were used as the controls. Tumor sizes were measured every 2 days after treatment. Remarkably, the tumors on the Fe-GA-PEG CPNs injected mice were completely eliminated one-day post NIR laser irradiation (Fig. 8a). In marked contrast, neither laser irradiation at this power density nor Fe-GA-PEG CPN injection by itself would affect the tumor development (Fig. 8c). While the mice in the three control groups showed average life spans of 16–18 days, the mice in the treated group (Fe-GA-PEG + Laser) were tumor-free after treatment and survived over 30 days without a single death (Fig. 8b). Our results suggested that Fe-GA-PEG CPNs are a powerful agent for *in vivo* photothermal ablation of cancer cells.

Despite the absence of visible *in vitro* toxicity of Fe-GA-PEG CPNs to some different cell lines, their potential *in vivo* toxicity to animals is still an important question to be addressed. We carefully supervised the behaviors of Fe-GA-PEG CPN injected (20 mg kg^{-1}) Balb/c mice in our experiments after photothermal tumor ablation, and noticed no discernible sign of toxic effects within 30 days. No abnormalities in body weight, eating, drinking, grooming, activity, exploratory behavior, urination, or neurological status were observed. The mice were then sacrificed at day 30 for careful necropsy, which uncovered no significant abnormality in the major organs. The major organs of the mice were sliced and stained with hematoxylin and eosin (H&E) for histology analysis (Fig. 8d), revealing no noticeable organ damage or inflammatory lesion in all the major organs of the mice 60 days after PTT treatment.

Conclusion

In summary, ultra-small Fe-GA CPNs with uniform sizes were successfully synthesized *via* a simple method. The synthesized Fe-GA-PEG CPNs could be labeled with a ^{64}Cu isotope upon simple mixing without the need for chelators, enabling *in vivo* PET imaging, which together with *in vivo* PA/MR multi-modal imaging, revealed the high tumor uptake of Fe-GA-PEG CPNs after i.v. injection. Finally, without showing notable *in vivo* toxicity, highly efficient photothermal destruction was achieved after i.v. injection of Fe-GA-PEG CPNs.

The following features make such Fe-GA-PEG a promising nanoscale theranostic agent: (1) these CNPs are formed purely by biocompatible components, ensuring their safe *in vivo* use. (2) The fabrication process of such Fe-GA-PEG appears to be rather simple and straightforward. (3) Based on a rather simple system, multiple imaging and therapy functions are well-integrated within Fe-GA-PEG CPNs, which are particularly promising for applications in multimodal imaging-guided cancer therapy.

Supplementary Material

Refer to Web version on PubMed Central for supplementary material.

Acknowledgments

This work was partially supported by the National Natural Science Foundation of China (51572180, 51525203, 51302180), the National Research Programs from the Ministry of Science and Technology (MOST) of China (2016YFA0201200), and the Post-doctoral science foundation of China (2013 M531400, 2014 T70542). This work was also partly supported by the University of Wisconsin–Madison, the National Institutes of Health (NIBIB/NCI 1R01CA169365 and P30CA014520), and the American Cancer Society (125246-RSG-13-099-01-CCE).

References

1. Topalian SL, Taube JM, Anders RA, Pardoll DM. Nat Rev Cancer. 2016; 16:275–287. [PubMed: 27079802]
2. Murtaza M, Dawson SJ, Tsui DW, Gale D, Forshew T, Piskorz AM, Parkinson C, Chin SF, Kingsbury Z, Wong AS. Nature. 2013; 497:108–112. [PubMed: 23563269]
3. Kroemer G, Galluzzi L, Kepp O, Zitvogel L. Annu Rev Immunol. 2013; 31:51–72. [PubMed: 23157435]
4. Cheng L, Wang C, Feng L, Yang K, Liu Z. Chem Rev. 2014; 114:10869–10939. [PubMed: 25260098]
5. Schumacher TN, Schreiber RD. Science. 2015; 348:69–74. [PubMed: 25838375]
6. Kamkaew A, Lim SH, Lee HB, Kiew LV, Chung LY, Burgess K. Chem Soc Rev. 2013; 42:77–88. [PubMed: 23014776]
7. Yang K, Zhang S, Zhang G, Sun X, Lee ST, Liu Z. Nano Lett. 2010; 10:3318–3323. [PubMed: 20684528]
8. Liu Z, Chen K, Davis C, Sherlock S, Cao Q, Chen X, Dai H. Cancer Res. 2008; 68:6652–6660. [PubMed: 18701489]
9. Huang X, El-Sayed IH, Qian W, El-Sayed MA. J Am Chem Soc. 2006; 128:2115–2120. [PubMed: 16464114]
10. O'Neal DP, Hirsch LR, Halas NJ, Payne JD, West JL. Cancer Lett. 2004; 209:171–176. [PubMed: 15159019]
11. Huang P, Lin J, Li W, Rong P, Wang Z, Wang S, Wang X, Sun X, Aronova M, Niu G. Angew Chem, Int Ed. 2013; 125:14208–14214.
12. Cheng L, Yang K, Li Y, Chen J, Wang C, Shao M, Lee ST, Liu Z. Angew Chem, Int Ed. 2011; 123:7523–7528.
13. Hu M, Chen J, Li ZY, Au L, Hartland GV, Li X, Marquez M, Xia Y. Chem Soc Rev. 2006; 35:1084–1094. [PubMed: 17057837]
14. Lal S, Clare SE, Halas NJ. Acc Chem Res. 2008; 41:1842–1851. [PubMed: 19053240]
15. Skrabalak SE, Chen J, Sun Y, Lu X, Au L, CoBLEY LM, Xia Y. Acc Chem Res. 2008; 41:1587–1595. [PubMed: 18570442]
16. Wang Y, Black KC, Luehmann H, Li W, Zhang Y, Cai X, Wan D, Liu SY, Li M, Kim P. ACS Nano. 2013; 7:2068–2077. [PubMed: 23383982]

17. Sun Z, Xie H, Tang S, Yu XF, Guo Z, Shao J, Zhang H, Huang H, Wang H, Chu PK. Angew Chem, Int Ed. 2015; 127:11688–11692.
18. Wang H, Yang X, Shao W, Chen S, Xie J, Zhang X, Wang J, Xie Y. J Am Chem Soc. 2015; 137:11376–11382. [PubMed: 26284535]
19. Cheng L, Liu J, Gu X, Gong H, Shi X, Liu T, Wang C, Wang X, Liu G, Xing H. Adv Mater. 2014; 26:1886–1893. [PubMed: 24375758]
20. Liu J, Zheng X, Yan L, Zhou L, Tian G, Yin W, Wang L, Liu Y, Hu Z, Gu Z. ACS Nano. 2015; 9:696–707. [PubMed: 25561009]
21. Yong Y, Cheng X, Bao T, Zu M, Yan L, Yin W, Ge C, Wang D, Gu Z, Zhao Y. ACS Nano. 2015; 9:12451–12463. [PubMed: 26495962]
22. Cheng L, Yuan C, Shen S, Yi X, Gong H, Yang K, Liu Z. ACS Nano. 2015; 9:11090–11101. [PubMed: 26445029]
23. Chen Y, Wang L, Shi J. Nano Today. 2016; 11:292–308.
24. Song G, Wang Q, Wang Y, Lv G, Li C, Zou R, Chen Z, Qin Z, Huo K, Hu R. Adv Funct Mater. 2013; 23:4281–4292.
25. Cheng L, Yang K, Chen Q, Liu Z. ACS Nano. 2012; 6:5605–5613. [PubMed: 22616847]
26. Yang J, Choi J, Bang D, Kim E, Lim EK, Park H, Suh JS, Lee K, Yoo KH, Kim EK. Angew Chem, Int Ed. 2011; 50:441–444.
27. Fan W, Bu W, Shen B, He Q, Cui Z, Liu Y, Zheng X, Zhao K, Shi J. Adv Mater. 2015; 27:4155–4161. [PubMed: 26058562]
28. Liang X, Li Y, Li X, Jing L, Deng Z, Yue X, Li C, Dai Z. Adv Funct Mater. 2015; 25:1451–1462.
29. Shen J, Zhao L, Han G. Adv Drug Delivery Rev. 2013; 65:744–755.
30. Chu KF, Dupuy DE. Nat Rev Cancer. 2014; 14:199–208. [PubMed: 24561446]
31. Horcajada P, Chalati T, Serre C, Gillet B, Sebrie C, Baati T, Eubank JF, Heurtaux D, Clayette P, Kreuz C, Chang JS, Hwang YK, Marsaud V, Bories PN, Cynober L, Gil S, Ferey G, Couvreur P, Gref R. Nat Mater. 2010; 9:172–178. [PubMed: 20010827]
32. Rocca JD, Liu D, Lin W. Acc Chem Res. 2011; 44:957–968. [PubMed: 21648429]
33. Horcajada P, Gref R, Baati T, Allan PK, Maurin G, Couvreur P, Férey G, Morris RE, Serre C. Chem Rev. 2011; 112:1232–1268. [PubMed: 22168547]
34. Rieter WJ, Pott KM, Taylor KM, Lin W. J Am Chem Soc. 2008; 130:11584–11585. [PubMed: 18686947]
35. Chen D, Yang D, Dougherty CA, Lu W, Wu H, He X, Cai T, Van Dort ME, Ross BD, Hong H. ACS Nano. 2017; 11:4315–4327. [PubMed: 28345871]
36. Zhang C, Bu W, Ni D, Zuo C, Cheng C, Li Q, Zhang L, Wang Z, Shi J. J Am Chem Soc. 2016; 138:8156–8164. [PubMed: 27264421]
37. Zhang C, Bu W, Ni D, Zhang S, Li Q, Yao Z, Zhang J, Yao H, Wang Z, Shi J. Angew Chem, Int Ed. 2016; 128:2141–2146.
38. Yang Y, Liu J, Liang C, Feng L, Fu T, Dong Z, Chao Y, Li Y, Lu G, Chen M, Liu Z. ACS Nano. 2016; 10:2774–2781. [PubMed: 26799993]
39. Liu J, Chen Q, Zhu W, Yi X, Yang Y, Dong Z, Liu Z. Adv Funct Mater. 2017; doi: 10.1002/adfm.201605926
40. Liu F, He X, Chen H, Zhang J, Zhang H, Wang Z. Nat Commun. 2015; 6:8003. [PubMed: 26245151]
41. Zeng J, Cheng M, Wang Y, Wen L, Chen L, Li Z, Wu Y, Gao M, Chai Z. Adv Healthcare Mater. 2016; 5:772–780.
42. Cheng L, Shen S, Shi S, Yi Y, Wang X, Song G, Yang K, Liu G, Barnhart TE, Cai W. Adv Funct Mater. 2016; 26:2185–2197. [PubMed: 27110230]
43. Sun X, Cai W, Chen X. Acc Chem Res. 2015; 48:286–294. [PubMed: 25635467]
44. Shi S, Xu C, Yang K, Goel S, Valdovinos HF, Luo H, Ehlerding EB, England CG, Cheng L, Chen F. Angew Chem, Int Ed. 2017; 129:2935–2938.
45. Kim C, Favazza C, Wang LV. Chem Rev. 2010; 110:2756–2782. [PubMed: 20210338]

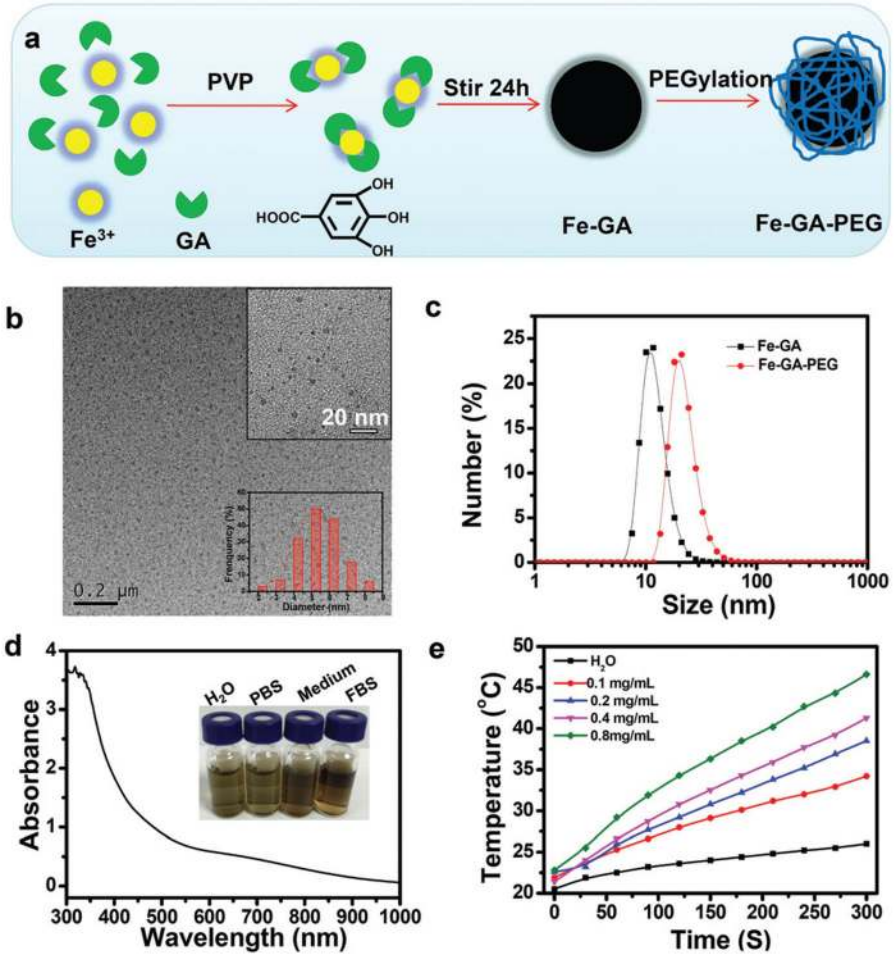

Fig. 1.

Synthesis and characterization of Fe-GA-PEG CPNs. (a) A scheme showing CPN synthesis and PEGylation. (b) TEM images of ultra-small Fe-GA-PEG CPNs. Inset: High-resolution TEM image (upper right) and the statistical size distribution (bottom right) of Fe-GA-PEG CPNs. (c) The hydrodynamic diameters (HDs) of Fe-GA and Fe-GA-PEG CPNs in water. (d) UV-vis-NIR absorbance spectra of Fe-GA-PEG CPNs in water (0.05 mg mL^{-1}). Inset: A photograph of Fe-GA-PEG CPNs dispersed in water, phosphate buffered saline (PBS), cell culture medium, and fetal bovine serum (FBS). (e) The photothermal heating curves of Fe-GA-PEG CPNs with different concentrations under 808 nm laser irradiation at the power density of 0.8 W cm^{-2}.

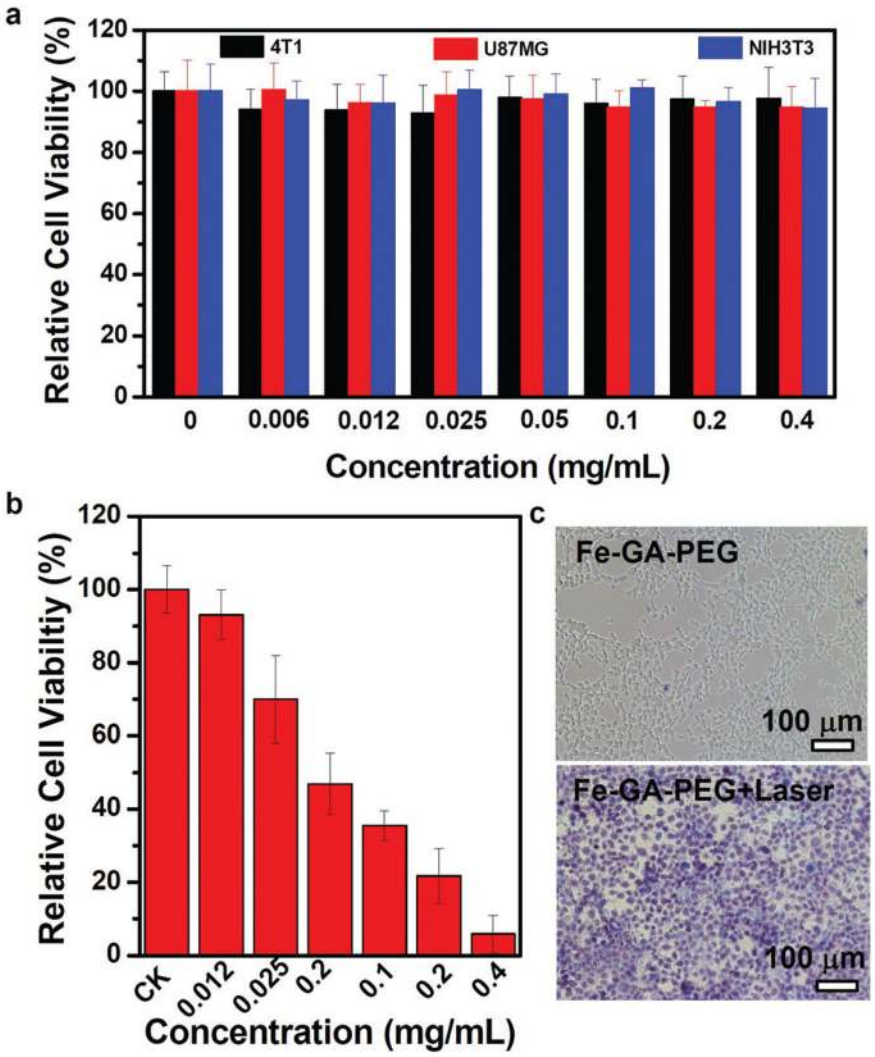

Fig. 2.

In vitro toxicity and photothermal therapy. (a) Relative viabilities of different types of cells after being incubated with various concentrations of Fe-GA-PEG CPNs for 24 h. Fe-GA-PEG CPNs exhibited no appreciable negative effect on the viability of cells. (b) Relative viabilities of 4T1 cells treated by Fe-GA-PEG CPNs with different concentrations under 808 nm light irradiation for 5 min $n = 4$. (c) Trypan blue stained 4T1 cells with PBS or Fe-GA-PEG CPN incubation after being exposed to the 808 nm laser, with blue indicating dead cells.

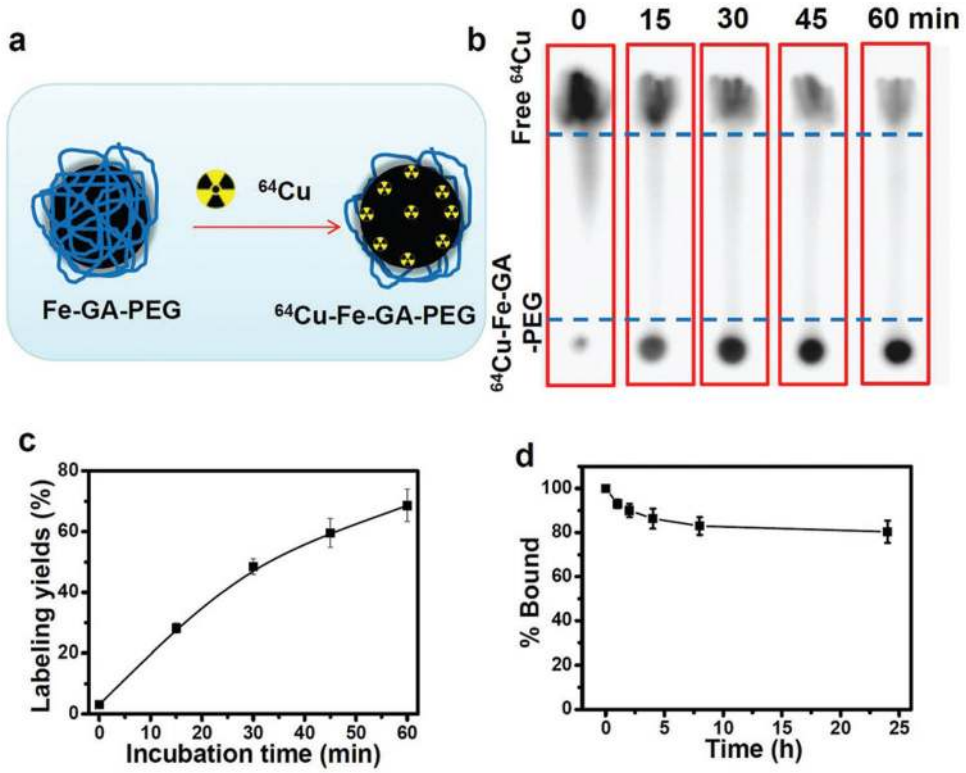

Fig. 3.

Chelator-free ^{64}Cu labeled Fe-GA-PEG CPNs. (a) A scheme showing ^{64}Cu labeling on Fe-GA-PEG CPNs *via* a chelator-free manner. (b) Thin-layer chromatography (TLC) plates of Fe-GA-PEG CPNs at various time points after mixing ^{64}Cu with Fe-GA-PEG CPNs. (c) Quantified labeling yields of ^{64}Cu on Fe-GA-PEG CPNs at various time points after incubation ($n = 3$). (d) Stability test of ^{64}Cu labeling on Fe-GA-PEG CPNs after incubation in serum at 37 °C for different periods of time. Error bars were based standard deviations (SD) of three samples at each time point.

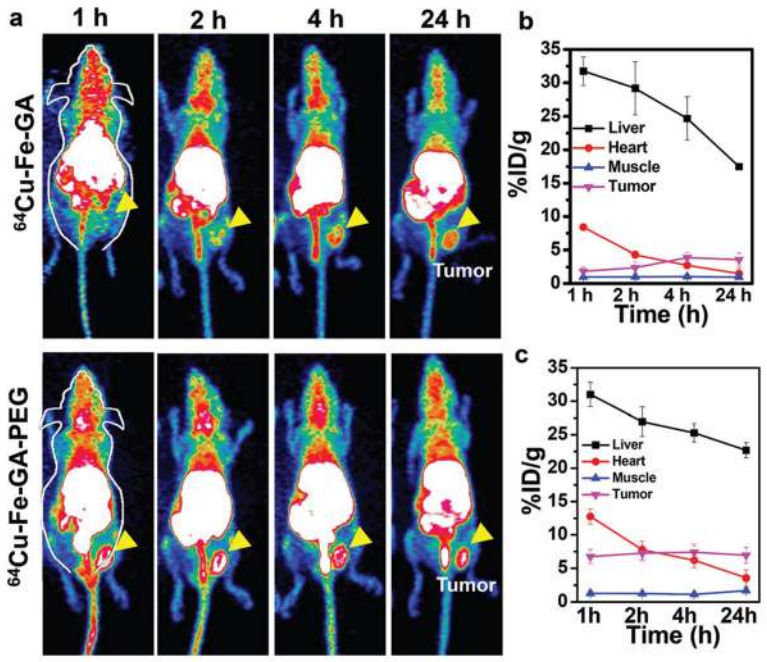

Fig. 4.

In vivo PET imaging. (a) PET images of 4T1 tumor-bearing mice taken at various time points (1, 2, 4, and 24 h) post intravenous injection of ^{64}Cu-Fe-GA CPNs without (upper) or with PEG (bottom) coating. The yellow triangle symbol represented the tumor site. (b & c) Quantification of ^{64}Cu-Fe-GA CPNs (b) and ^{64}Cu-Fe-GA-PEG CPNs (c) uptake in the liver, blood, 4T1 tumor, and muscle at various time points. The unit is the percentage of injected dose per gram of tissue (%ID g^{-1}, $n = 3$).

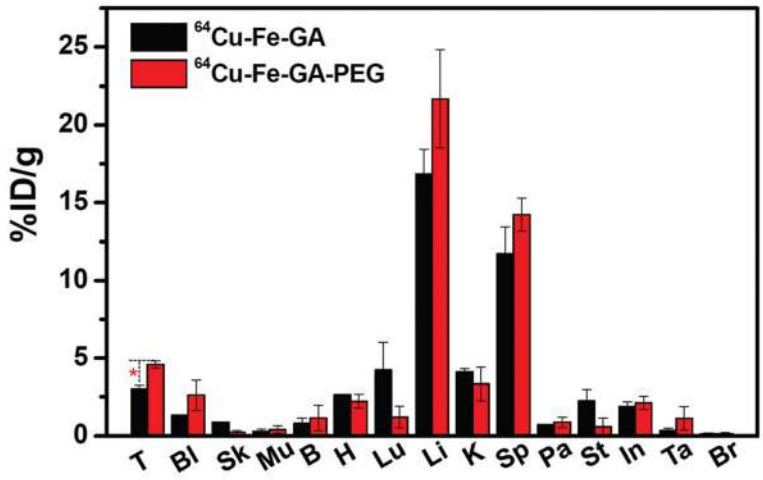

Fig. 5.

Biodistribution of ^{64}Cu-Fe-GA and ^{64}Cu-Fe-GA-PEG CPNs at 24 h after i.v. injection into 4T1 tumor-bearing mice as determined by ^{64}Cu radioactivity measurement in various organs and tissues (T: tumor; Bl: blood; Sk: skin; Mu: muscle; B: bone; H: heart; Lu: lung; Li: liver; K: kidney; Sp: spleen; Pa: pancreas; St: stomach; In: intestine; Ta: tail; Br: brain). Error bars were based on the standard error of the mean (SEM) of triplicate samples. Statistical analysis was performed using the student's two-tailed *t* test: $*p < 0.05$.

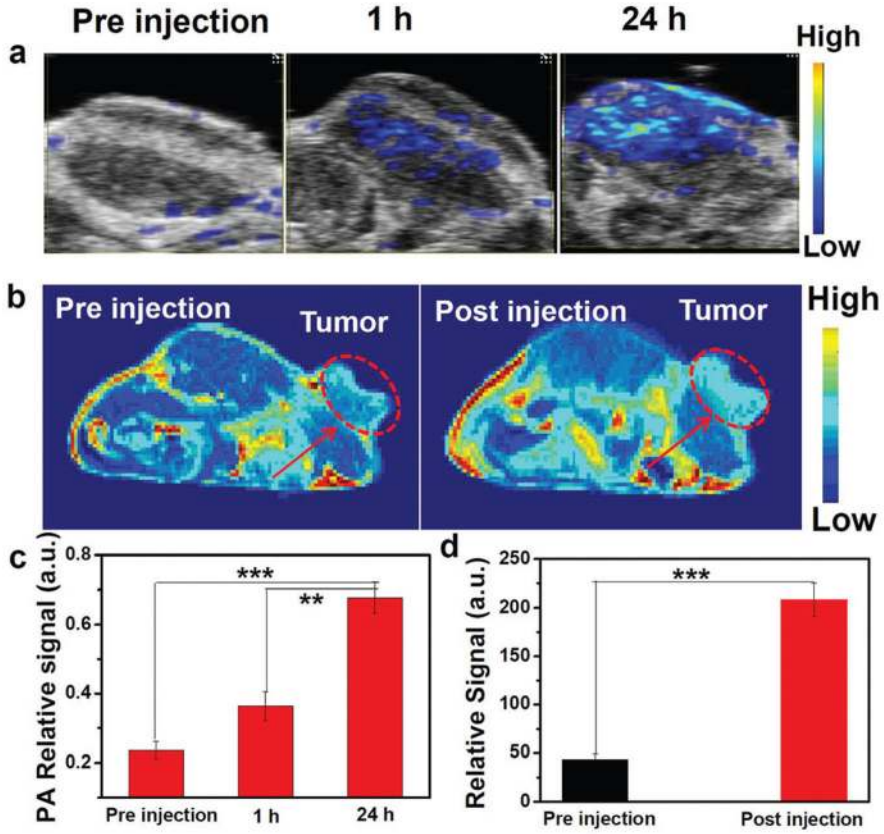

Fig. 6.

In vivo dual-modal imaging. (a) *In vivo* PAT images of tumors on mice after injection with Fe-GA-PEG CPNs taken at different time points (0 h, 1 h, and 24 h). (b) T_1-Weighted MR images of mice before and 24 h after i.v. injection with Fe-GA-PEG CPNs. (c & d) Quantified PA signals (c) and MR signals (d) of tumors from mice after i.v. injection of Fe-GA-PEG CPNs based on the above imaging data. Statistical analysis was performed using the student's two-tailed *t* test: $*p < 0.05$, $**p < 0.01$, and $***p < 0.001$.

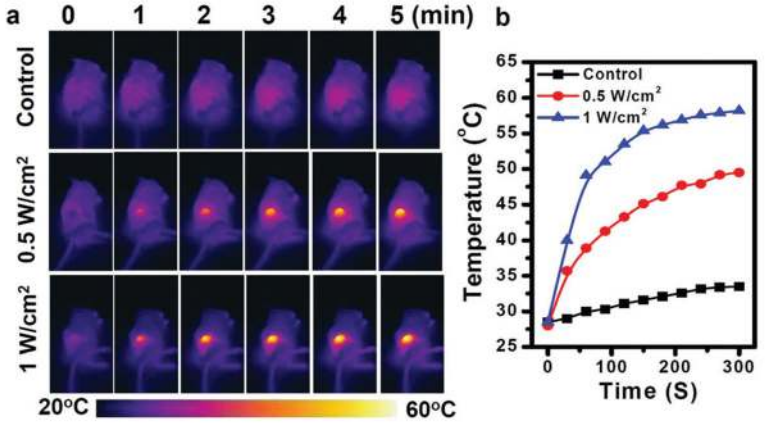

Fig. 7.

In vivo photothermal heating. (a) IR thermal images of 4T1 tumor-bearing mice without or with i.v. injection of Fe-GA-PEG CPNs (dose = 20 mg kg^{-1}, irradiated at 24 h p.i.), under the 808 nm laser irradiation with different power intensities (0.5 and 1 W cm^{-2}) taken at different time intervals. (b) Temperature changes of tumors monitored by using an IR thermal camera during laser irradiation based on IR thermal images.

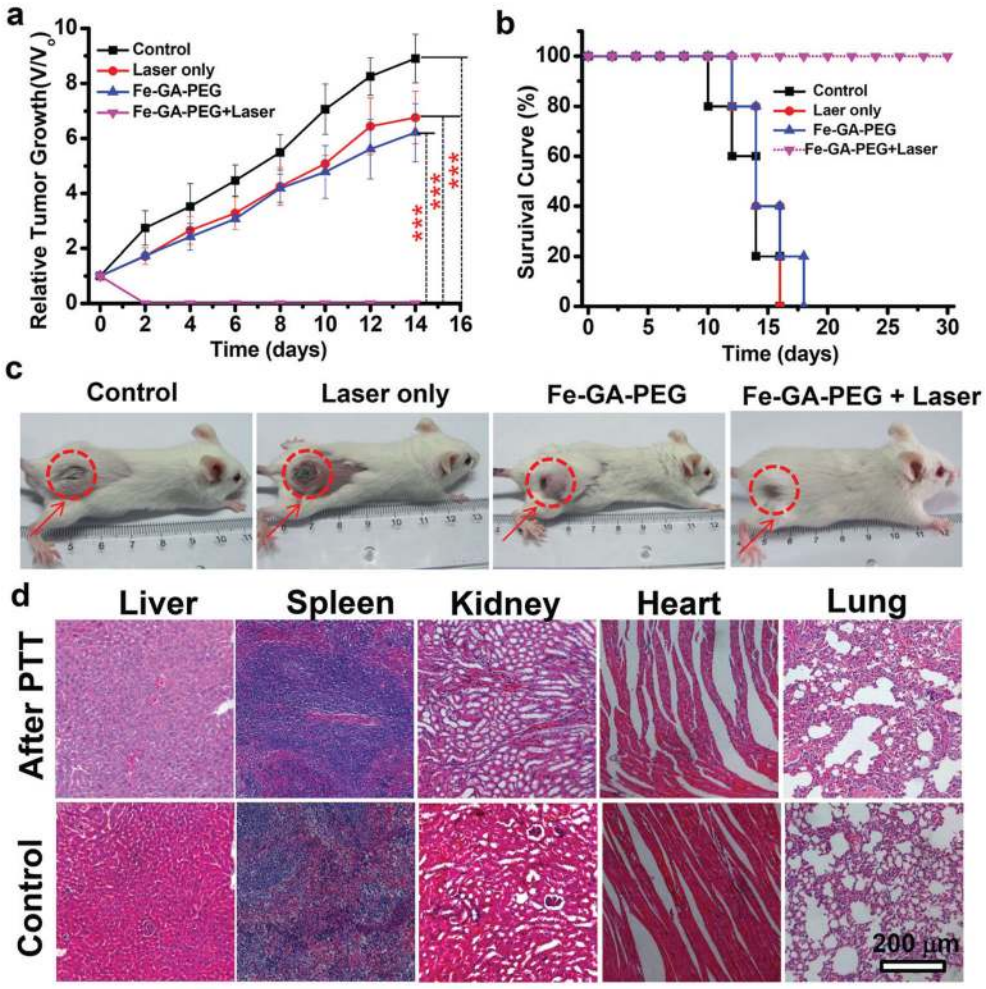

Fig. 8.

In vivo photothermal therapy. (a) Tumor growth curves of different groups of mice after various treatments indicated. For the treatment group, five mice injected with Fe-GA-PEG CPNs at 24 h p.i. were exposed to the 808 nm laser (1 W cm^{-2}, 5 min). Another three groups of mice were used as controls: untreated (control, $n = 5$); laser only without Fe-GA-PEG CPNs injection (laser only, $n = 5$); Fe-GA-PEG CPNs injected but without laser irradiation (Fe-GA-PEG CPNs, $n = 5$). Error bars were based on SD. Statistical analysis was performed using the student's two-tailed t test: $^*p < 0.05$, $^{**}p < 0.01$, and $^{***}p < 0.001$. (b) Survival curves of mice after various treatments as indicated in (a). (c) Representative photographs of mice from different groups taken at the 14th day. (d) H&E stained images of major organs. Fe-GA-PEG CPNs injected mice that survived after PTT (with tumors eliminated) were sacrificed 30 days after treatment. Untreated healthy mice were used as the control. No obvious abnormality was observed in major organs including, liver, spleen, kidney, heart, and lung.